Road Materials and Pavement Design

ISSN: (Print) (Online) Journal homepage: https://www.tandfonline.com/loi/trmp20

Effect of principal stress rotation on deformation behavior of dense sand–clay mixtures

Halil Ibrahim Fedakar, Cassandra J. Rutherford & Bora Cetin

To cite this article: Halil Ibrahim Fedakar, Cassandra J. Rutherford & Bora Cetin (2021): Effect of principal stress rotation on deformation behavior of dense sand–clay mixtures, Road Materials and Pavement Design, DOI: 10.1080/14680629.2021.1948908

To link to this article: https://doi.org/10.1080/14680629.2021.1948908

ROAD MATERIALS AND PAVEMENT DESIGN
https://doi.org/10.1080/14680629.2021.1948908

Taylor & Francis
Taylor & Francis Group

Effect of principal stress rotation on deformation behavior of dense sand–clay mixtures

Halil Ibrahim Fedakar [a], Cassandra J. Rutherford [b] and Bora Cetin [c]

[a]Department of Civil Engineering, Abdullah Gul University, Kayseri, Turkey; [b]Department of Civil, Construction and Environmental Engineering, Iowa State University, Ames, IA, USA; [c]Department of Civil and Environmental Engineering, Michigan State University, East Lansing, MI, USA

ABSTRACT

This paper investigated the deformation behaviour of *K*-consolidated sand–clay mixtures through cyclic triaxial (CT) and hollow cylinder (CHC) tests. The sand–clay mixtures contained 0%, 5%, 10% and 20% clay by weight and were prepared at a relative density of 75%. Clay inclusion caused an increase in the permanent axial strain of mixtures (0.075% to 5% in CT and 0.186% to 5% in CHC), while a relatively insignificant increase in permanent axial strain was observed in the CT specimens containing 5% and 10% clay (0.075% to 1.299%). However, all CHC specimens with clay failed ($\varepsilon_z \geq 5\%$). It was also observed that shear strain development of sand is significantly influenced by clay inclusion (0.096–2.241%) in CHC tests. Test results clearly show that the effect of a principal stress rotation should be taken into account to better estimate the deformation behaviour of sand–clay mixtures under repetitive traffic loads.

ARTICLE HISTORY
Received 11 January 2021
Accepted 23 June 2021

KEYWORDS
Hollow cylinder test; principal stress rotation; triaxial test; deformation; sand–clay mixture

1. Introduction

Traffic loads cause an excessive permanent deformation in the pavement foundation layers (base, subbase and subgrade soil layers). This effect is more significant for flexible pavements. It is well known that permanent deformation development may adversely affect the performance of an entire pavement structure (i.e. pavement rutting) and cause major maintenance costs (Cetin et al., 2014; Fedakar et al., 2020; Haider et al., 2014; Korkiala-Tanttu & Dawson, 2007; Li et al., 2019; Puppala et al., 1999, 2009). The degree of permanent deformation in a pavement structure depends on several factors. These factors include vehicle speeds, number of load cycles as well as soil properties and environmental factors. Due to the advances in vehicle technology and rapid urbanization in recent years, pavement structures have been subjected to higher traffic loads. As a result of this, the development of permanent deformation has become one of the main pavement engineering problems that have been encountered. The permanent deformation develops as a result of the accumulation of irrecoverable strains in pavement foundation layers (Cai et al., 2015; Puppala et al., 1999). To minimise these effects on a pavement structure, engineering designs aim to lower the strains developed in soil layers by traffic loading to the negligible values (Guo et al., 2018). This can be achieved by a better understanding of the behaviour of soils/geomaterials under repeated traffic loads. Therefore, in the last decade, the deformation behaviour of soils/geomaterials under repeated traffic loads has become the primary interest of many studies (Alnedawi et al., 2018, 2021; Cai et al., 2015, 2017, 2018; Cetin et al., 2014; Cui, 2018; Frost et al., 2004; Georgiannou & Konstadinou, 2014; Guimarães et al., 2019; Guo et al., 2016, 2018;

CONTACT Halil Ibrahim Fedakar halilibrahim.fedakar@agu.edu.tr

Haider et al., 2014; Kim & Kim, 2007; Li et al., 2019; Noolu et al., 2019; Qian et al., 2016; Saberian et al., 2019; Saberian & Li, 2019; Shen et al., 2017; Yang et al., 2019).

As shown in Figure 1, a moving wheel load results in a change in both magnitude and direction of principal stresses acting on a soil particle which is known as the principal stress rotation. Soil layers beneath an asphalt layer are imposed to a heart-shaped (or cardioid-shaped) stress path due to traffic loading (Cai et al., 2015; Fedakar et al., 2020; Gao et al., 2017; Guo et al., 2016; Qian et al., 2016). A heart-shaped stress path includes axial stress and shear stress in a deviatoric stress space and induces a principal stress rotation. Previous studies investigating the deformation behaviour of soils under long-term traffic loads have commonly used cyclic triaxial (CT) tests to simulate the actual field wheel loading in a laboratory test setup (Alnedawi et al., 2018, 2021; Cui, 2018; Frost et al., 2004; Guimarães et al., 2019; Kim & Kim, 2007; Li et al., 2019; Noolu et al., 2019; Saberian et al., 2019; Saberian & Li, 2019). However, these tests are restricted to keep any two of the three principal stresses equal, while the angle of major principal stress with respect to vertical is either 0^o or 90^o (Cai et al., 2018; Guo et al., 2018). Furthermore, a conventional triaxial testing apparatus is designed to apply only axial stress on a specimen. Thus, it is not capable of imposing a principal stress rotation and heart-shaped stress path, which causes the effect of traffic loading on the deformation behaviour of soils/geomaterials to be underestimated. To overcome these limitations of a conventional triaxial test, more advanced testing systems are required to simulate actual field traffic loads better in a laboratory test setup.

A hollow cylinder apparatus allows four degrees of load components to be controlled independently. Therefore, it can simulate a principal stress rotation induced by complex stress paths for the specimens that are in a suitable geometry and do not exhibit large strain (Cai et al., 2015; Guo et al., 2018). Due to these capabilities, hollow cylinder tests have been successfully conducted in imposing a better simulated principal stress rotation on soil specimens in the last decade (Cai et al., 2015, 2017, 2018; Georgiannou & Konstadinou, 2014; Guo et al., 2016, 2018; Qian et al., 2016; Yang et al., 2019). Previous studies clearly indicated that the principal stress rotation and heart-shaped stress path, resulting from a vehicle wheel loading, may have a significant impact on the deformation behaviour of soils. The degree of this effect depends on soil types as well as the stress states that specimens are subjected to. A subgrade layer is a native soil that generally consists of soils with different types and particle sizes. The materials with a coarser fraction of coarse-grained (sand, in general) and a lower amount of fine-grained soil can also be used as a subbase material in a transportation infrastructure. The permanent deformation in pavement foundation layers (i.e. subbase and subgrade) due to traffic loading contributes to pavement rutting significantly (Cai, 2010; Cai et al., 2015; Chai & Miura, 2002; Puppala et al., 1999). Therefore, the soils with various types and particle sizes should be tested to better understand the deformation accumulation in a pavement structure. While there have been studies examining the behaviour of soils (i.e. sand, and soft clay materials) under traffic loads through cyclic hollow cylinder (CHC) tests (Cai et al., 2015; Cai et al., 2017, 2018; Georgiannou & Konstadinou, 2014; Guo et al., 2016,

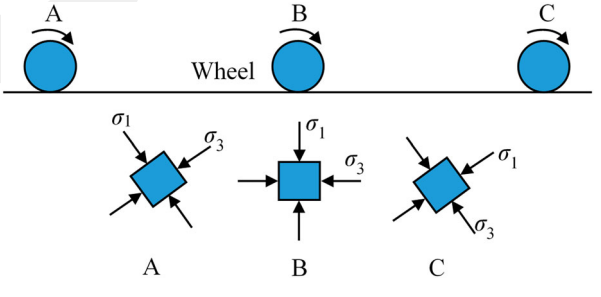

Figure 1. Rotation of principal stresses acting on a soil particle under a moving wheel load (Guo et al., 2016).

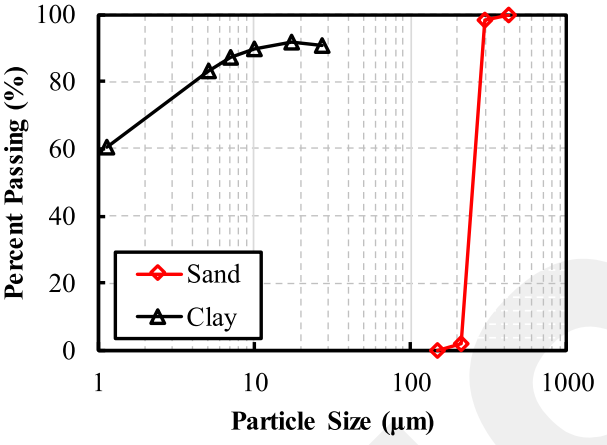

Figure 2. Particle size distributions of both sand and clay used.

2018; Qian et al., 2016; Yang et al., 2019), there is limited information about the permanent deformation behaviour of sand–clay mixtures under the principal stress rotation induced by a heart-shaped stress path.

According to the previous studies mentioned above, a principal stress rotation induced by a moving wheel load may have a significant impact on deformation characteristics of soils used in pavement foundation layers and therefore should be taken into account in pavement applications. These studies investigated the deformation performances of clay and sand specimens under repeated traffic loads. In a pavement construction, sand–clay mixtures containing clay at low amounts are also used in pavement foundation layers (particularly subbase and subgrade layers). However, there are limited studies that investigated the deformation behaviour of sand–clay mixtures with low clay contents under a heart-shaped stress path. To address this gap in existing literature, the effect of a principal stress rotation on the deformation and stress–strain behaviours of sand–clay mixtures was investigated in this study. To achieve this goal, a series of CT and CHC tests were conducted on sand–clay specimens that contained clay at 0%, 5%, 10% and 20% by weight. During testing, both axial load and torque were cyclically and simultaneously applied on CHC specimens to simulate a heart-shaped stress path more accurately while only cyclic axial load was applied on CT specimens for a CT stress path. To better understand the effect of a principal stress rotation and a heart-shaped stress path on the strain developing in sand–clay mixtures, the results by CHC tests were compared to those by CT tests.

2. Materials and methods

2.1. Testing materials and specimen preparation

Four sand–clay mixtures consisting of varying amounts of Ottawa 50/70 sand and pulverised EPK Kaolin clay were used in this study. The sand was supplied from EMD Millipore Sigma Corporation, USA. Its coefficient of uniformity (C_u) and coefficient of curvature (C_c) were 1.22 and 0.97, respectively. In addition, its minimum and maximum void ratios were 0.61 and 0.78, respectively. It was classified as poorly graded sand (SP) according to the Unified Soil Classification System (USCS). The clay material used was supplied from Edgar Minerals, USA. Its liquid limit and plastic limit were 62% and 41%, respectively. It was classified as high plasticity clay (CH) according to the USCS. The specific gravities of both materials were 2.65. Their particle size distributions are given in Figure 2.

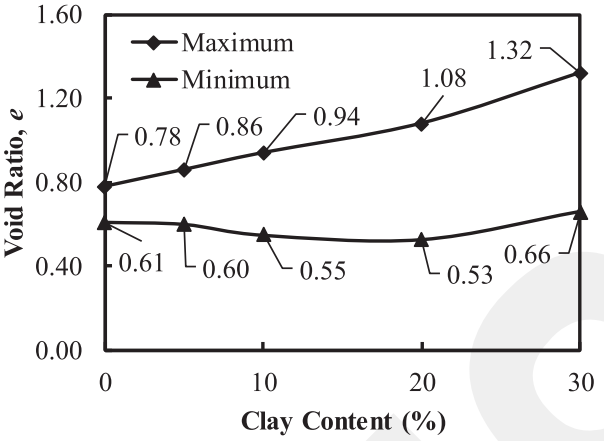

Figure 3. Variation of minimum and maximum void ratios with clay contents.

It is well known that clay materials have undesirable properties such as compressibility, swelling and hydraulic conductivity for uses in subbase layers. For this reason, an upper limit for the clay content was determined according to 'the critical fine content' by Simpson and Evans (2016) where a minimum void ratio occurs without displacing sand grains. Therefore, 0%, 5%, 10%, 20% and 30% clay by weight was added to sand and then, their minimum and maximum void ratios were determined. Figure 3 shows the minimum and maximum void ratios of all sand–clay mixtures. The minimum void ratio (0.53) was observed with the mixture that had 20% clay (Figure 3). Therefore, the inclusion rate of the clay was limited to 20%.

All specimens were prepared in a hollow cylindrical shape and were homogenous in their dimensions that were 200 mm in height, 60 mm in internal diameter, and 100 mm in outer diameter. These dimensions were selected to minimise stress non-uniformities. In addition, the centre of the specimen was not influenced by the boundary conditions due to these selected dimensions (Cai et al., 2015; Hight et al., 1983; Vaid et al., 1990). High vacuum grease was applied along the edges of parts of the outer mould for a better sealing during mounting. A vacuum pressure of approximately 50 kPa was applied to get rid of the air between the outer mould and the outer membrane. During the mixture preparation, dry sand and clay materials were manually mixed at predetermined rates (0%, 5%, 10% and 20% clay by weight) to obtain a uniform mixture. It should be noted that the dry deposition method was adopted for the specimen preparation in this study. The sand–clay mixtures were poured into a hollow cylinder space between inner and outer moulds in five layers by using a funnel. During this procedure, the falling height was kept at zero and extreme care was taken to avoid the segregation. All mixtures were prepared at an initial relative density of 75% to represent the dense state. To achieve the target density ($D_r = 75\%$), the mixtures were dry tamped to the target height at each layer. Then, a top cap was put on the specimen and the tubing of the testing machine involving outer chamber to specimen, inner chamber to specimen and back pressure controller to specimen was connected. Thereafter, a vacuum pressure of 25 kPa was applied from the bottom to hold the specimen and to make the inner/outer membranes fully adhere to the mould walls. Applying vacuum pressure at this stage sometimes may lead clogging of bottom porous stone by fine particles. Thus, dry-tamping method was preferred in this study. After placing the specimen in the testing apparatus, inner/outer chambers were filled with de-aired water. 30 kPa of inner/outer cell pressures were applied to the specimen immediately and the applied vacuum pressure was released by opening the valves. During the flushing process, de-aired water was circulated into the specimen from bottom to top. This process was continued until the air was removed from the inside of the specimen.

2.2. Testing procedures

In this study, both CT and CHC tests had the following 3 stages: (1) saturation, (2) *K*-consolidation, and (3) shearing. Although the plain strain condition can be achieved in a hollow cylinder test by applying different inner/outer cell pressures (Shibuya, 1988; Pradhan et al., 1988), variations in stress and strain can occur across the specimen's wall when a hollow cylindrical specimen is subjected to either torque or different inner/outer cell pressures (Hight et al., 1983). This cause of stress and strain non-uniformities are minimised or reduced by keeping inner/outer cell pressures equal (Cai et al., 2015; Guo et al., 2018; Hight et al., 1983; Mamou, 2013; Mamou et al., 2018; Qian et al., 2016). Therefore, inner/outer cell pressures were kept equal throughout the CT and CHC tests of this study. At the saturation stage, inner/outer cell pressures and back pressure were incrementally increased to 320 and 300 kPa, respectively, by keeping the effective confining pressure (20 kPa) constant. This was done until the specimen was saturated. The Skempton's pore water pressure parameter of *B* was utilized to determine whether the specimen was saturated. All specimens had *B* values greater than 0.95 by the end of saturation stage, indicating that the saturation stage was completed. During the consolidation stage, all specimens were anisotropically consolidated with $K = 0.5$. Back pressure was kept constant (300 kPa) during this stage. Firstly, the vertical stress (σ_z) was enhanced from 320 kPa to 340 kPa to obtain $K = 0.5$, while inner/outer cell pressures were kept constant (320 kPa). Then, the vertical stress and inner/outer cell pressures were simultaneously increased from 340 kPa to 360 kPa and from 320 kPa to 330 kPa, respectively. The specimens were anisotropically consolidated under these pressures. After this stage, all CT and CHC specimens were sheared under undrained conditions according to the testing plan presented in Table 1. CT5 and CHC5 in Table 1 represent CT and CHC tests applied on specimens with 5% clay, respectively. In addition, the expressions of η, *CVSR*, *f*, and *N* denote the cyclic torsional stress ratio ($\tau_{z\theta}{}^{amp}/\sigma_z{}^{amp}$), cyclic vertical stress ratio ($\sigma_z{}^{amp}/2p'_0$), frequency, and number of loading cycles, respectively. The p'_0 in *CVSR* is the initial effective mean normal stress ($=(\sigma'_{z0}+\sigma'_{r0}+\sigma'_{\theta 0})/3$) ($\sigma'_{z0}$, σ'_{r0}, and $\sigma'_{\theta 0}$ represent initial effective vertical stress, radial stress, and circumferential stress, respectively) (Cai et al., 2015). While CT tests involved only cyclic axial stress (30 kPa), CHC tests involved both cyclic axial stress (30 kPa) and torsional shear stress (10 kPa) to mimic a heart-shaped stress path (Table 1). The loading frequency was set to 1 Hz in both CT and CHC tests (Chazallon et al., 2006; Guo et al., 2018; Ishihara, 1996). Every specimen was subjected to 10,000 of loading cycles to represent the long-term traffic loading. Test data were saved for every 1 cycle to be able to analyse the test results within each cycle. In addition, 50 data points were taken per cycle to better characterise the waveforms and stress paths.

2.3. Testing apparatus and stress–strain states in a hollow cylinder specimen

All tests in this study were conducted by using a hollow cylinder apparatus (HCA). This testing apparatus tests a specimen with 100 mm in outer diameter (d_o), 60 mm in inner diameter (d_i) and 200 mm in

Table 1. Summary of experimental plan.

Test ID	Sand (%)	Clay (%)	Tests	$\sigma_z{}^{amp}$ (kPa)	$\tau_{z\theta}{}^{amp}$ (kPa)	η	*CVSR*	*f* (Hz)	*N*
CT0	100	0	CT	30	0	0	0.125	1	10,000
CT5	95	5	CT	30	0	0	0.125	1	10,000
CT10	90	10	CT	30	0	0	0.125	1	10,000
CT20	80	20	CT	30	0	0	0.125	1	10,000
CHC0	100	0	CHC	30	10	1/3	0.125	1	10,000
CHC5	95	5	CHC	30	10	1/3	0.125	1	10,000
CHC10	90	10	CHC	30	10	1/3	0.125	1	10,000
CHC20	80	20	CHC	30	10	1/3	0.125	1	10,000

Note: CT and CHC represent cyclic triaxial and hollow cylinder tests, respectively; CT0 indicates the cyclic triaxial test on the specimen containing 0% clay; $\sigma_z{}^{amp}$ is the amplitude of cyclic axial stress; $\tau_{z\theta}{}^{amp}$ is the amplitude of cyclic shear stress; η is cyclic torsional stress ratio ($\tau_{z\theta}^{amp}/\sigma_z^{amp}$); *CVSR* is cyclic vertical stress ratio ($\sigma_z^{amp}/2p'_0$); ***f*** is frequency; ***N*** is number of load cycles.

height (H). According to Hight et al. (1983), the stress uniformity developed in a hollow cylinder specimen can be tolerable up to $d_i/d_o \geq 0.6$, and $H/d_o > 0.6$. An HCA is equipped with an independent control of four degrees of load components and therefore, can simulate the principal stress rotation due to complex stress paths (Cai et al., 2015; Guo et al., 2018; Wang et al., 2018). The axial and rotational actuators applied axial load and torque on the specimen, respectively. The applied axial load and torque were measured by a combined of load and torque transducers that were mounted on top of the specimen. The vertical deformation and rotational angle were measured by encoders mounted on the actuator motor shafts (Cai et al., 2015; Guo et al., 2018). Digital controllers were used to regulate inner/outer cell and back pressures through de-aired water and to measure the volume changes in inner/outer chambers and specimen. More detailed descriptions about this testing system are available in Cai et al. (2015), Gräbe and Clayton (2009), Guo et al. (2018), Wang et al. (2018), and Xiong et al. (2016).

An HCA system imposes a vertical load (W), a torque (M_T), and inner/outer cell pressures (p_i and p_o, respectively) on a specimen and also enables them to be controlled independently. In a hollow cylinder specimen, a vertical stress (σ_z), a shear stress ($\tau_{z\theta}$), a circumferential stress (σ_θ) and a radial stress (σ_r) can be developed by these external loads and pressures (Cai et al., 2015). In addition, a specimen may undergo the following strain components under these stress states: Vertical strain (ε_z), shear strain ($\gamma_{z\theta}$), circumferential strain (ε_θ), and radial strain (ε_r). Furthermore, the concept of principal stress (i.e. major principal stress (σ_1), intermediate principal stress (σ_2), and minor principal stress (σ_3)) can be used to define the stress state of a specimen. The stress and strain states developed in a hollow cylinder specimen are illustrated in Figure 4. The rotational angle (α) of the major principal stress to the vertical stress due to the principal stress rotation is shown in Figure 4. The equations by Hight et al. (1983) in Table 2 were used in this study to calculate the stress and strain states (Figure 4). The expressions of r_o, r_i, ΔH, u_o, u_i, θ, ε_1, ε_2 and ε_3 in Table 2 represent outer radius, inner radius, vertical displacement, outer radius movement of the wall of the specimen, inner radius movement of the wall of the specimen, rotational displacement, major principal strain, intermediate principal strain and minor principal strain, respectively.

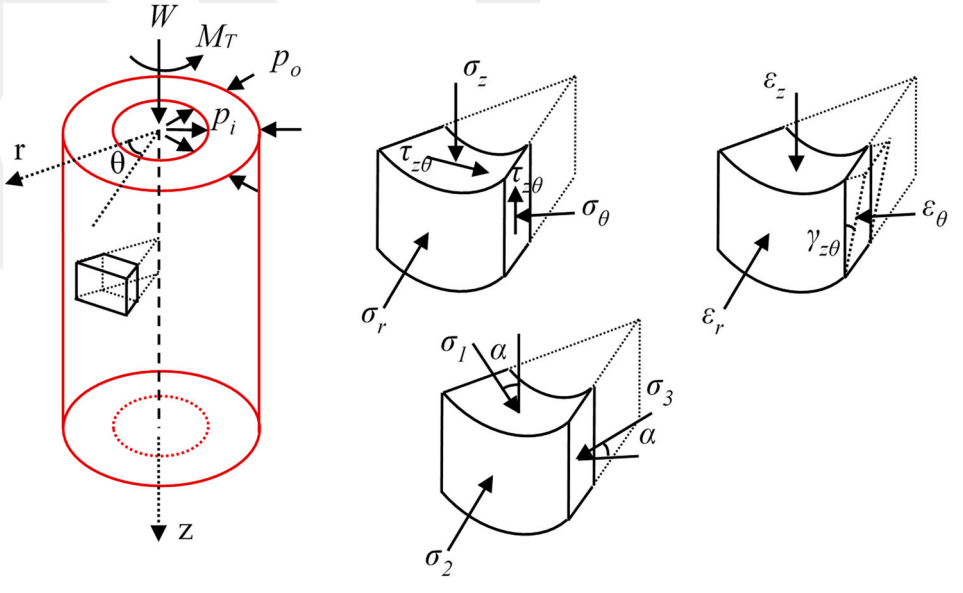

Figure 4. Stress and strain states in a hollow cylinder specimen (Guo et al., 2016).

Table 2. Equations for the average stress and strain components

Component	Stress	Strain
Vertical	$\sigma_z = \frac{W}{\pi(r_0^2 - r_i^2)} + \frac{p_o r_0^2 - p_i r_i^2}{(r_0^2 - r_i^2)}$	$\varepsilon_z = \frac{\Delta H}{H}$
Circumferential	$\sigma_\theta = \frac{p_o r_o - p_i r_i}{(r_o - r_i)}$	$\varepsilon_\theta = \frac{u_o + u_i}{r_o + r_i}$
Radial	$\sigma_r = \frac{p_o r_o + p_i r_i}{(r_o + r_i)}$	$\varepsilon_r = \frac{u_o - u_i}{r_o - r_i}$
Shear	$\tau_{z\theta} = \frac{M_T}{2}\left[\frac{3}{2\pi(r_o^3 - r_i^3)} + \frac{4(r_o^3 - r_i^3)}{3\pi(r_o^2 - r_i^2)(r_o^4 - r_i^4)}\right]$	$\gamma_{z\theta} = \frac{\theta(r_o^3 - r_i^3)}{3H(r_o^2 - r_i^2)}$
Major principal	$\sigma_1 = \frac{\sigma_z + \sigma_\theta}{2} + \sqrt{\left(\frac{\sigma_z - \sigma_\theta}{2}\right)^2 + \tau_{z\theta}^2}$	$\varepsilon_1 = \frac{\varepsilon_z + \varepsilon_\theta}{2} + \sqrt{\left(\frac{\varepsilon_z - \varepsilon_\theta}{2}\right)^2 + \gamma_{z\theta}^2}$
Intermediate principal	$\sigma_2 = \sigma_r$	$\varepsilon_2 = \varepsilon_r$
Minor principal	$\sigma_3 = \frac{\sigma_z + \sigma_\theta}{2} - \sqrt{\left(\frac{\sigma_z - \sigma_\theta}{2}\right)^2 + \tau_{z\theta}^2}$	$\varepsilon_3 = \frac{\varepsilon_z + \varepsilon_\theta}{2} - \sqrt{\left(\frac{\varepsilon_z - \varepsilon_\theta}{2}\right)^2 + \gamma_{z\theta}^2}$

Notes: σ_z: vertical stress; σ_θ: circumferential stress; σ_r: radial stress; $\tau_{z\theta}$: torsional shear stress; σ_1: major principal stress; σ_2: intermediate principal stress; σ_3: minor principal stress; W: vertical load; M_T: torque; p_o: outer cell pressure; p_i: inner cell pressure; r_o: outer radius; r_i: inner radius; ε_z: vertical strain; ε_θ: circumferential strain; ε_r: radial strain; ε_1: major principal strain; ε_2: intermediate principal strain; ε_3: minor principal strain; $\gamma_{z\theta}$: shear strain; H: initial height of the specimen; ΔH: vertical displacement; u_o: outer radius movement of the wall of the specimen; u_i: inner radius movement of the wall of the specimen; θ: rotational displacement.

2.4. Heart-Shaped stress path

A heart-shaped stress path in a deviatoric stress space ($\tau_{z\theta}$ to (σ_z-σ_θ)/2) is imposed on soils in pavement foundation layers due to a moving wheel load. A specimen is subjected to both torsional shear stress ($\tau_{z\theta}$) and vertical stress (σ_z) as well as circumferential stress (σ_θ) during the shearing stage of a CHC test to simulate such a stress path in a laboratory test setup. Figure 5 illustrates a heart-shaped stress path and its stress waveforms. The stress expressions in Figure 5 are presented in terms of cyclic stress. Figure 5(a) shows the amplitudes of torsional shear stress and vertical stress in a loading cycle ($\tau_{z\theta}{}^{amp}$ and $\sigma_z{}^{amp}$). According to Figure 5(b), the torsional shear stress is not equal to the deviatoric stress in magnitude. The expression of 'α' in Figure 5(b) denotes the angle of cyclic major principal stress (or major principal stress increment) with respect to the vertical axis. The angle of α rotates between $-\pi/2$ and $+\pi/2$ (Cai et al., 2015). As stated before, the inner/outer cell pressures were kept constant and equal in all tests to minimise the stress non-uniformities. Moreover, these stresses remained constant and equal while shearing the specimens. Consequently, both torsional shear stress and vertical stress with the following predefined waveforms (Equations (1) and (2)) were cyclically applied on all CHC specimens.

$$\sigma_z^{cyc} = 0.5\sigma_z^{amp}\left[\frac{1}{2}cos(2\omega t) - cos(\omega t) + \frac{1}{2}\right] \quad (1)$$

$$\tau_{z\theta}^{cyc} = 0.77\tau_{z\theta}^{amp}\left[sin(\omega t) - \frac{1}{2}sin(2\omega t)\right] \quad (2)$$

where t is the elapsed time and $\omega = 2\pi/T$ (T is the period and 1 s in this study).

CT tests were also conducted to better understand the effect of a principal stress rotation induced by a heart-shaped stress path. Only vertical stress with a predefined waveform in Equation (1) was

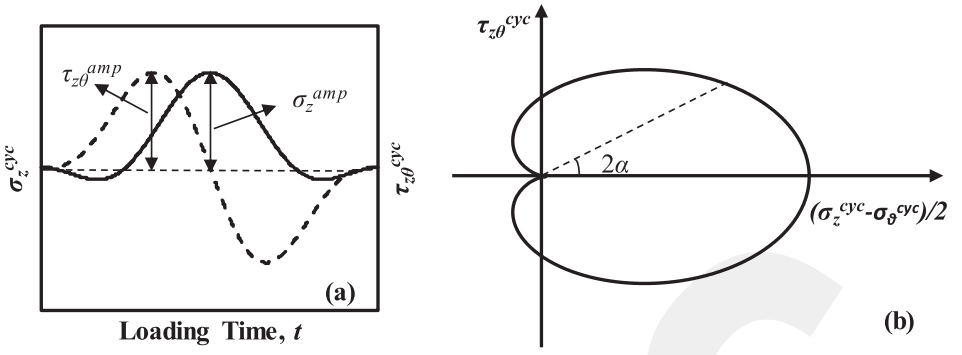

Figure 5. Schematic diagram of (a) waveforms of cyclic stresses and (b) a heart-shaped stress path.

cyclically applied to simulate the loading condition of a conventional triaxial test where no torsional shear stress is applied.

2.5. Stress corrections for the membrane forces

All CT and CHC tests on the sand–clay mixtures were performed on the specimens which were enclosed by flexible membranes. However, the use of inner/outer membranes in these tests may affect the accuracy of the measured stresses (Saada, 1988). Therefore, in this study, the measured stress parameters (σ_z, σ_r, σ_θ, and $\tau_{z\theta}$) were corrected for the influences of the membrane forces induced by the inner/outer membranes according to Tatsuoka et al. (1986), Gräbe (2002), Mamou (2013) and Cai et al. (2015). Further information about the corrections for the membrane forces made in this study can be found in Tatsuoka et al. (1986), Gräbe (2002), Mamou (2013) and Cai et al. (2015).

2.6. Strain development

All soils/geomaterials used in pavement foundation layers undergo permanent strain and resilient strain under traffic loading. Total strain is defined as the sum of permanent strain and resilient strain. Figure 6 illustrates typical strains developed within a loading cycle (Guo et al., 2018). Test results were presented in terms of the development of axial (i.e. vertical) strain and shear strain in specimens and their stress–strain behaviours.

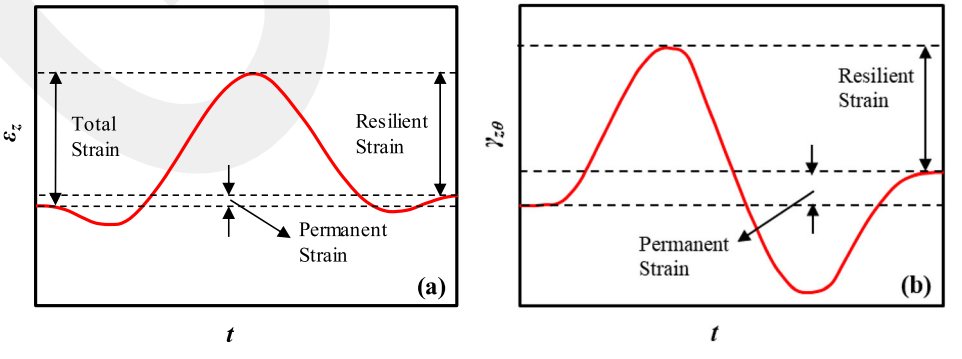

Figure 6. Typical strain development within a cycle due to (a) axial stress and (b) torsional shear stress (adapted from Guo et al., 2018).

3. Results and discussions

3.1. Stress paths

An example of the waveforms of vertical stress, torsional shear stress and stress paths applied to the specimens without clay and with 20% clay within a loading cycle is shown in Figure 7. Figure 7 also shows the target waveforms and stress paths within the dashed lines. The target waveforms for torsional shear stress and vertical stress are shown in red and black colours in Figures 7(a,c), respectively. In addition, the dashed lines in red and black colours in Figures 7(b,d) indicates the target stress paths for CT and CHC tests, respectively. Based on the results, it can be said that the measured waveforms for the stress parameters (torsional shear stress and vertical stress) match well with the target waveforms for the specimens without clay (Figure 7(a)). However, the specimens with 20% clay yielded lower peak values for both vertical stress and torsional shear stress in a cycle (Figure 7(c)). This can be due to the fact that the specimens with clay produced higher deformation during shearing. As for the stress path, it is expected that a CT test imposes a stress path in a straight line along the horizontal axis due to its loading condition where only vertical stress is cyclically applied. Unlike a CT test, a CHC test generates a stress path in a heart-shaped since both torsional shear and vertical stresses can be cyclically applied simultaneously. It is clear in Figures 7(b,d) that the CHC tests applied the heart-shaped stress path on the specimens. Furthermore, the CT tests produced a stress path in a straight line along the horizontal axis (Figures 7(b,d)). Results showed that the stress paths by CT and CHC tests match well with the target stress paths for the specimens without clay. However, due to higher deformation development

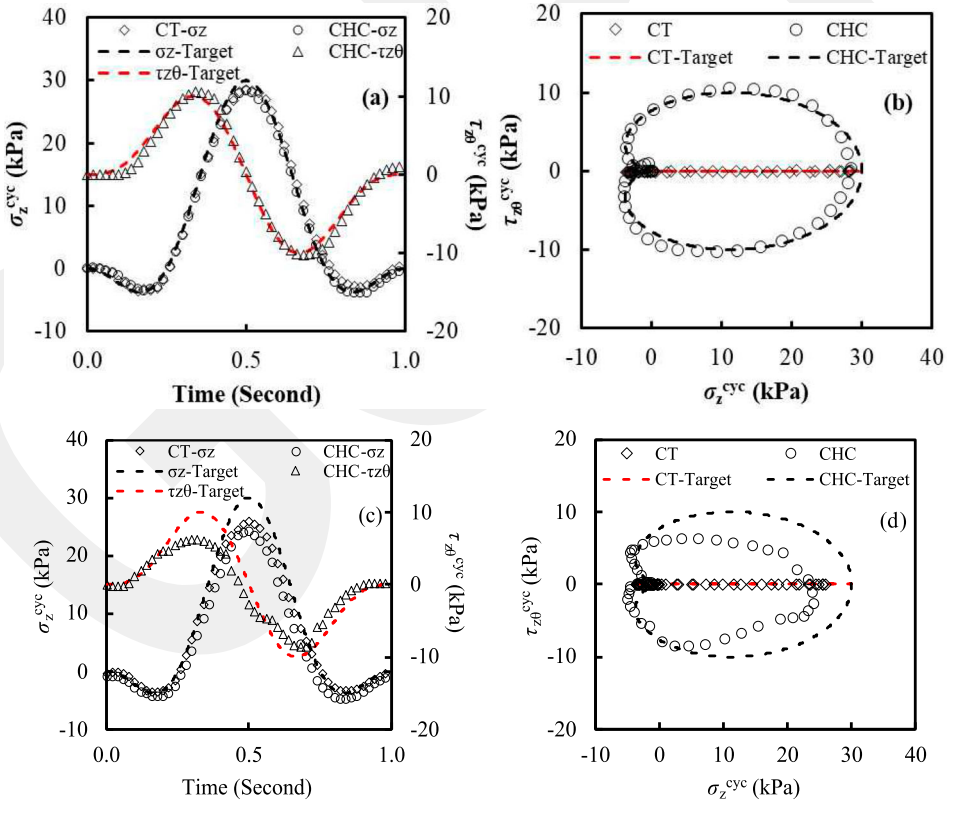

Figure 7. Examples of stress conditions in CT and CHC tests with and without clay: (a and b) Cyclic stress waveforms and corresponding stress paths for the specimens without clay; (c and d) cyclic stress waveforms and corresponding stress paths for the specimens with clay (20%).

in the specimens with clay, the stress paths with lower amplitudes were achieved in both tests (see Figure 7(d)). Nevertheless, the stress paths (particularly the heart-shaped stress path) imposed on the specimens with clay were determined to be satisfactory for this study. Test results of this study have an acceptable reliability for a better understanding of the effect of a heart-shaped stress path on the deformation behaviour of sand–clay mixtures.

3.2. Axial strain development

Figure 8 summarises a development of axial strain with the number of load cycles. In this figure, '0%C-CT' represents a specimen including 0% clay and subjected to a CT test. $\varepsilon_z \geq 5\%$ was used as a failure criterion in this paper (Cheung, 1994; Georgiannou & Konstadinou, 2014; Hyodo et al., 1991, 1994; Li et al., 2011; Qian et al., 2016; Shen et al., 2017; Vaid & Chern, 1983). Accordingly, the vertical axes in Figure 8 were limited to 5% for the specimens exhibiting high deformation ($\varepsilon_z \geq 5\%$). Figure 8 clearly shows that specimens that were particularly subjected to a CHC test failed ($\varepsilon_z \geq 5\%$) in earlier cycles ($N \leq 60$). Therefore, Figures 8(a, c, e, g) were plotted in logarithmic scales to more clearly show the quick accumulation of axial strains in earlier cycles.

It is speculated that sand particles rotate under a heart-shaped stress path and consequently, the sand specimen exhibits a higher vertical deformation. Nevertheless, a heart-shaped stress path causes a relative increase in vertical strain development of the specimen without clay (Figures 8(a,b)). A similar behaviour was also observed for Nanjing fine sand by Cai et al. (2015) who used *CVSR* values of 0.15, 0.25, 0.35 and 0.45. They also reported that the impact of a principal stress rotation on axial deformation of sand could become larger when the *CVSR* value increased. In this regard, the test results in Figures 8(a,b) imply that the used *CVSR* value ($=0.125$ in this study) is not high enough to cause accelerated axial strain accumulations in sand specimens (CT and CHC). In addition, the strain accumulations in sand specimens should be evaluated considering cyclic torsional stress ratio ($\eta = 0$ in CT tests and $\eta = 1/3$ in CHC tests) as well as *CVSR*. As given in Table 1, both sand specimens were subjected to same *CVSR* during tests. Thus, a relative increase in axial strain of sand specimen under a heart-shaped stress path could also be explained that the CHC tests of this study had a cyclic torsional stress ratio (η) greater than that used in the CT tests (see Table 1). Furthermore, from the evaluation of *CVSR* together with η, it can be speculated that the impact of η on axial strain behaviour of sand becomes less since lower torsional shear stress is applied for $\eta = 1/3$ under low *CVSR*. Figures 8(a,b) also show that the differences in axial strain due to the principal stress rotation increase with an increase in the number of load cycles.

Figures 8(c– h) show an axial strain development in the specimens with clay with the number of load cycles. It is well known that the presence of clay in sand yields an increase in the axial deformation of the soil matrix under load. The level of axial deformation is highly dependent on the clay content in sand–clay mixtures since clay has a higher compressibility. A similar behaviour was observed in CT test results. Figures 8(c–h) clearly show that a higher axial strain developed as the clay content increased. As mentioned earlier, the concept of 'the critical fine content' by Simpson and Evans (2016) was adopted to determine the clay contents to be used in this study. In this regard, the upper limit for clay inclusion was determined as 20% by weight where a minimum void ratio (0.53) was achieved. It is expected by the critical fine content that a sand–clay mixture containing up to 20% clay (including 20%) would carry the load without failure. According to Figures 8(c–f), the sand–clay mixtures containing 5%, and 10% clay carried the cyclic axial loads without failure (i.e. $\varepsilon_z < 5\%$) throughout 10,000 loading cycles. On the contrary, a quick axial deformation developed in a sand–clay mixture with 20% clay and consequently, the specimen failed at the 494th cycle.

According to the test results in Figures 8(c–h), unlike CT tests, all CHC specimens with clay failed under a heart-shaped stress path, which means that a level of axial strain developed in a sand–clay mixture (i.e. clay content $> 0\%$) is also influenced by stress ratios used in this study. So, although both CT and CHC specimens that contained clay at 5%, and 10% were sheared with same *CVSR*, the CHC specimens produced larger axial strains and failed in earlier cycles due to $\eta = 1/3$. This may be explained

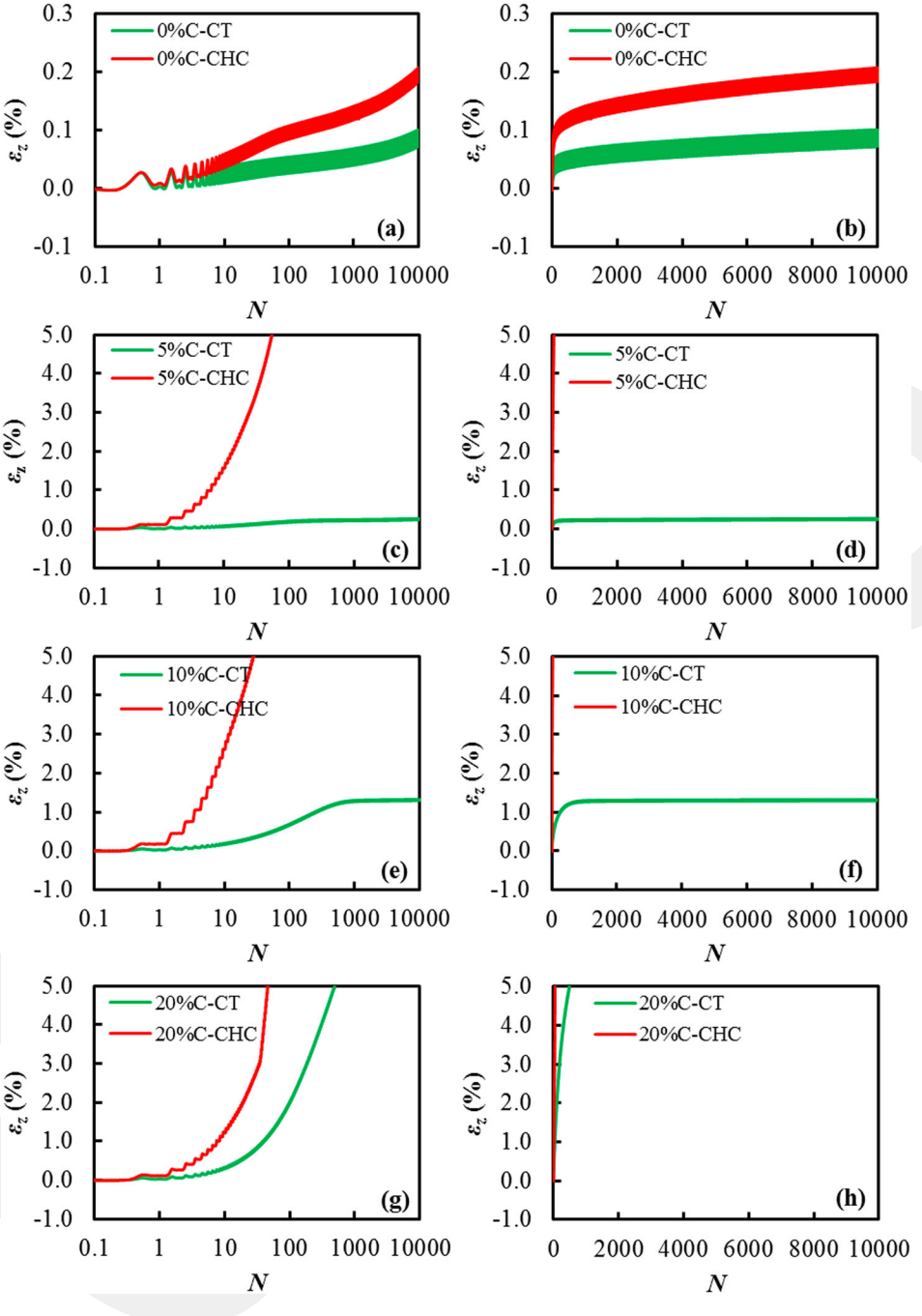

Figure 8. Axial strain versus number of load cycles for CT and CHC specimens: (a) 0% clay with logarithmic scale; (b) 0% clay without logarithmic scale; (c) 5% clay with logarithmic scale; (d) 5% clay without logarithmic scale; (e) 10% clay with logarithmic scale; (f) 10% clay without logarithmic scale; (g) 20% clay with logarithmic scale and (h) 20% clay without logarithmic scale.

that the torsional shear stress applied (10 kPa) exceeded shear strengths of these mixtures, causing their failure under cyclic loads. In addition, even though the specimens with 20% clay failed in both tests, axial strain developed more rapidly in the CHC specimen because of $\eta = 1/3$ and thus it failed earlier than the CT specimen. Due to stress ratios used ($CVSR = 0.125$, and $\eta = 1/3$), no impact of clay

contents on axial strain development was observed in CHC specimens. In other words, the effects of clay contents on axial strain behaviour of dense sand–clay mixtures could be more apparent under lower stress ratios. However, this is not within the scope of this study. Therefore, it was not tested. The axial strain behaviours of CHC specimens could also be explained that the contact areas between sand particles were reduced significantly due to the principal stress rotation. Thus, these areas and voids in the soil matrix were filled with clay particles instead. Based on these results, it can be claimed that the material properties of clay such as high compressibility may become a dominant parameter in sand–clay mixtures particularly under a heart-shaped stress path.

Figures 8(c–h) also show that some specimens produce an unstable pattern for axial strain development, which results in a quicker failure as a result of a sharp increase in axial strain accumulation. An overall evaluation of the results in Figures 8(c–h) indicates that a principal stress rotation can influence the behaviour of soils more than clay content, particularly at high *CVSR* and η values. Furthermore, it is also expected that clay content may have a significant impact on soil behaviour as the *CVSR* and η decrease. The axial strain developments in sand–clay mixtures within a single cycle are presented in Figure 9. Figure 9 clearly shows that the addition of clay at low rates (i.e. $\leq$ 20% by weight) results in a considerable increase in permanent deformation of sand under the principal stress rotation. Figures 8(a–h) also indicate that a permanent axial strain accumulates cumulatively resulting in high axial strain development as expected under longer loading conditions such as traffic loads. Figures 8(a–h) show that cyclic triaxial tests not including PSR with sudden 90-degree changes in the principal stress direction underestimate the axial strain development in dense sand–clay mixtures under long-term traffic loading. From an overall evaluation of the test results in Figures 8(a–h), it can also be concluded that a principal stress rotation induced by a heart-shaped stress path has a significant impact on permanent strain development in sand–clay mixtures, particularly in specimens with clay. Therefore, this

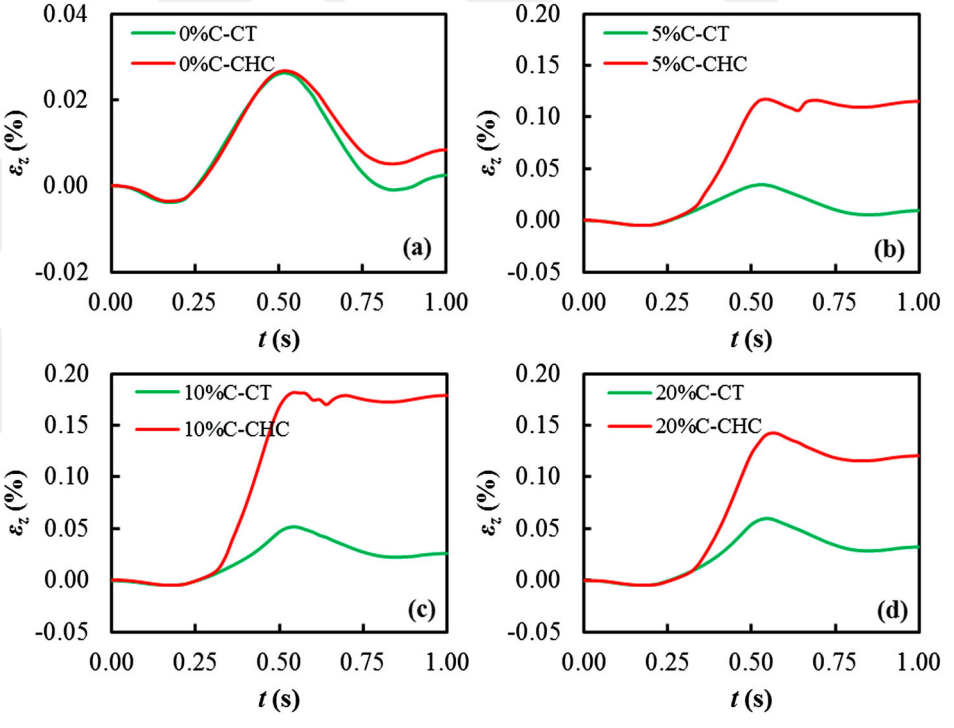

Figure 9. Axial strain development in CT and CHC specimens within one loading cycle: (a) 0% clay; (b) 5% clay; (c) 10% clay and (d) 20% clay.

impact needs to be taken into account to better understand the behaviour of sand–clay mixtures under traffic loading.

The deformation characteristics of soils under cyclic loads were also described by shakedown theory. Figure 8 presents test results for the shakedown behaviour of dense sand–clay mixtures. It is obvious in Figures 8(a-b) that the sand specimens exhibited plastic creep (i.e. a type of shakedown) behaviour in which the increment rate of permanent strain firstly enhanced rapidly ($N < 1000$) and then the permanent strain continued to develop slightly with increasing number of load cycles. Unlike the sand specimens, plastic shakedown and ratcheting behaviours were observed in the specimens including clay depending on the clay contents and stress paths (Figures 8(c–h)). In plastic shakedown behaviour, a specimen tends to exhibit a stable axial strain behaviour under cyclic loads after a quick accumulation of axial strain in earlier cycles. In addition, plastic shakedown is preferable in soils used in subgrade layer (Qian et al., 2016). This type of behaviour was observed in CT specimens including 5%, and 10% clay (Figures 8(c–f)). On the contrary of plastic shakedown, ratcheting behaviour should be avoided in practice since it indicates structural instability of soils under loads. In this study, it was determined that the specimens that failed exhibited ratcheting behaviour because of excessive permanent strain ($\varepsilon_z \geq 5\%$) (Figures 8(c–h)). From the results in Figure 8, it can be said that shakedown behaviour of sand is affected by clay inclusion and principal stress rotation. In CT tests of this study, ratcheting behaviour was achieved only for the specimen prepared with 20% clay content. On the other hand, the principal stress rotation by a heart-shaped stress path caused a ratcheting behaviour in all CHC specimens with clay (5%, 10% and 20%) implying that the principal stress rotation should be taken into consideration while evaluating shakedown behaviour of dense sand–clay mixtures containing clay under repeated traffic loads.

3.3. Axial stress–strain behavior

Figure 10 presents the results of axial stress–strain relationships of sand–clay mixtures during CT and CHC tests. It is shown that some of the failed specimens are subjected to lower axial stresses than the target amplitude. This is due to the large axial strain development in these specimens, influencing the parameters of σ_z in Table 2 (i.e. r_o and r_i). It can be seen that the axial stress–strain loops for all specimens shift to the right because they undergo an increasing axial strain under cyclic loads. In all the specimens without failure, most of axial strain due to cyclic loading developed within the first 1000 load cycles. With the increasing number of load cycles ($N > 1000$), these specimens produced less axial strain accumulation and reached a steady value for permanent strain at the end of load cycles (see Figures 10(a–c, and e)). On the contrary, the specimens with failure produced larger axial strains (i.e. $\varepsilon_z > 5\%$) at earlier load cycles and a steady value for permanent strain was not achieved (Figures 10d, 10f, and 10g-10 h). Thus, a gradual decrease in distance between each axial stress–strain loop was clearly observed in these specimens during testing. However, that is not clear in the CT specimen with 20% clay since it failed at a relatively higher load cycle compared to the CHC specimens containing clay. It is difficult to realise this behaviour (i.e. a gradual decrease in distance) in the specimens that did not fail owing to the higher number of load cycles (see Figures 10(a–c, and e)). Figures 10(d, f, and h) show the effect of clay contents on the axial stress–strain behaviour of the sand specimen during CHC tests. The CHC specimens containing 5% and 10% clay exhibited a gradually decrease in distance between each axial stress–strain loop as the number of load cycles increased. The CHC specimen with 20% clay also exhibited a similar behaviour up to $\varepsilon_z = 3\%$. However, after $\varepsilon_z = 3\%$, a gradual increase in distance between each axial stress–strain loop was observed in this specimen with the increasing number of load cycles. This behaviour can be explained that the 20% clay addition may result in less contact areas between sand particles after the 3% axial strain is reached. Consequently, a quicker development of axial strain takes place. It is also clear in Figures 10(c, e) that the specimens with 5% and 10% clay exhibit strain-hardening behaviour under cyclic loads during CT tests. This behaviour was also slightly observed in the specimens without clay (see Figures 10(a,b)). On the other hand, the failed specimens

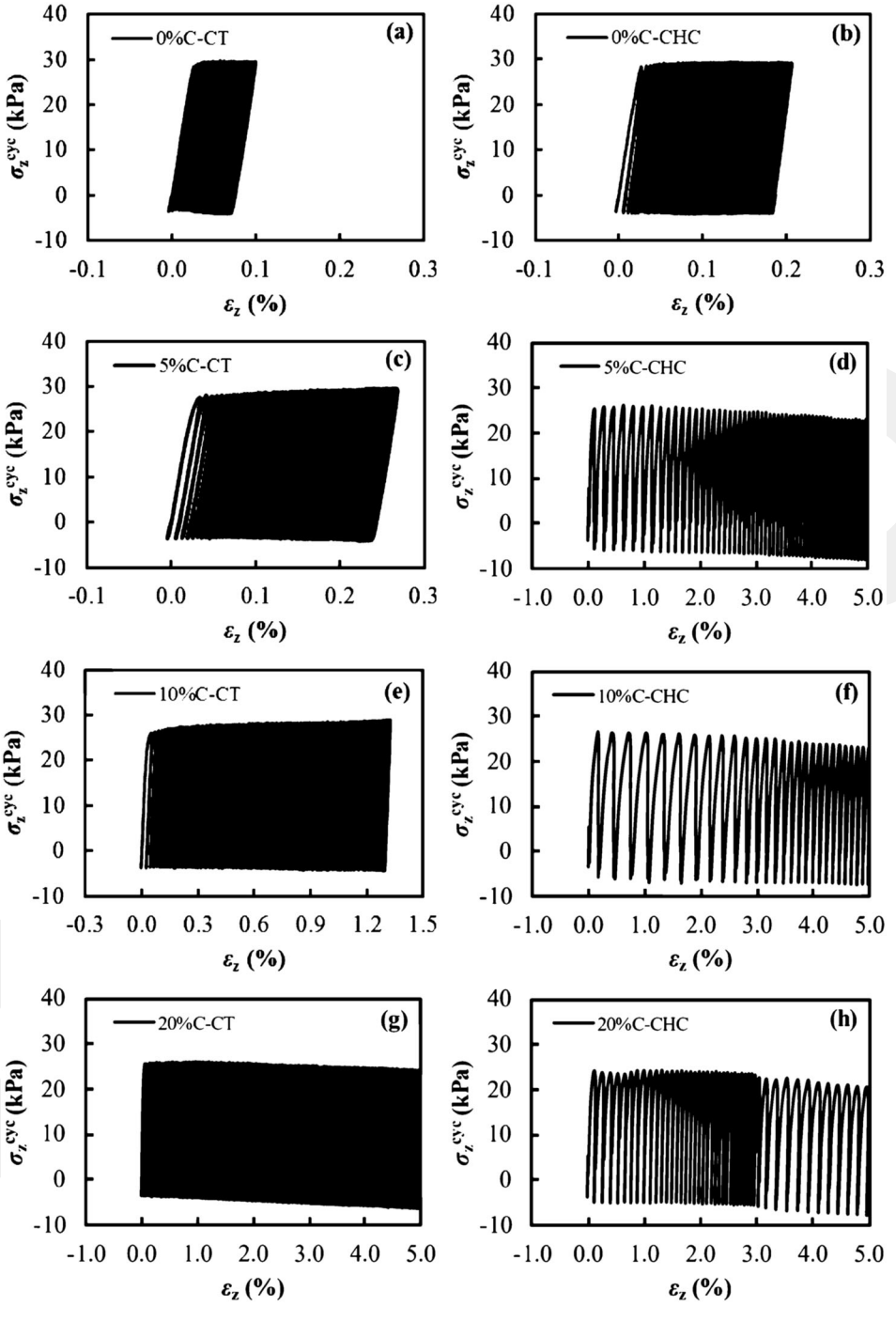

Figure 10. Axial stress versus axial strain for CT and CHC specimens: (a) CT-0% clay; (b) CHC-0% clay; (c) CT-5% clay; (d) CHC-5% clay; (e) CT-10% clay; (f) CHC-10% clay; (g) CT-20% clay and (h) CHC-20% clay.

exhibited strain-softening behaviour under cyclic loads. This behaviour was more obvious in the specimens that were subjected to the principal stress rotation, indicating the effect of a heart-shaped stress path on axial strain development in sand–clay mixtures. However, the strain-softening behaviour in '20%C-CT' could be attributed to the fact that the clay particles became more dominant in the mixture

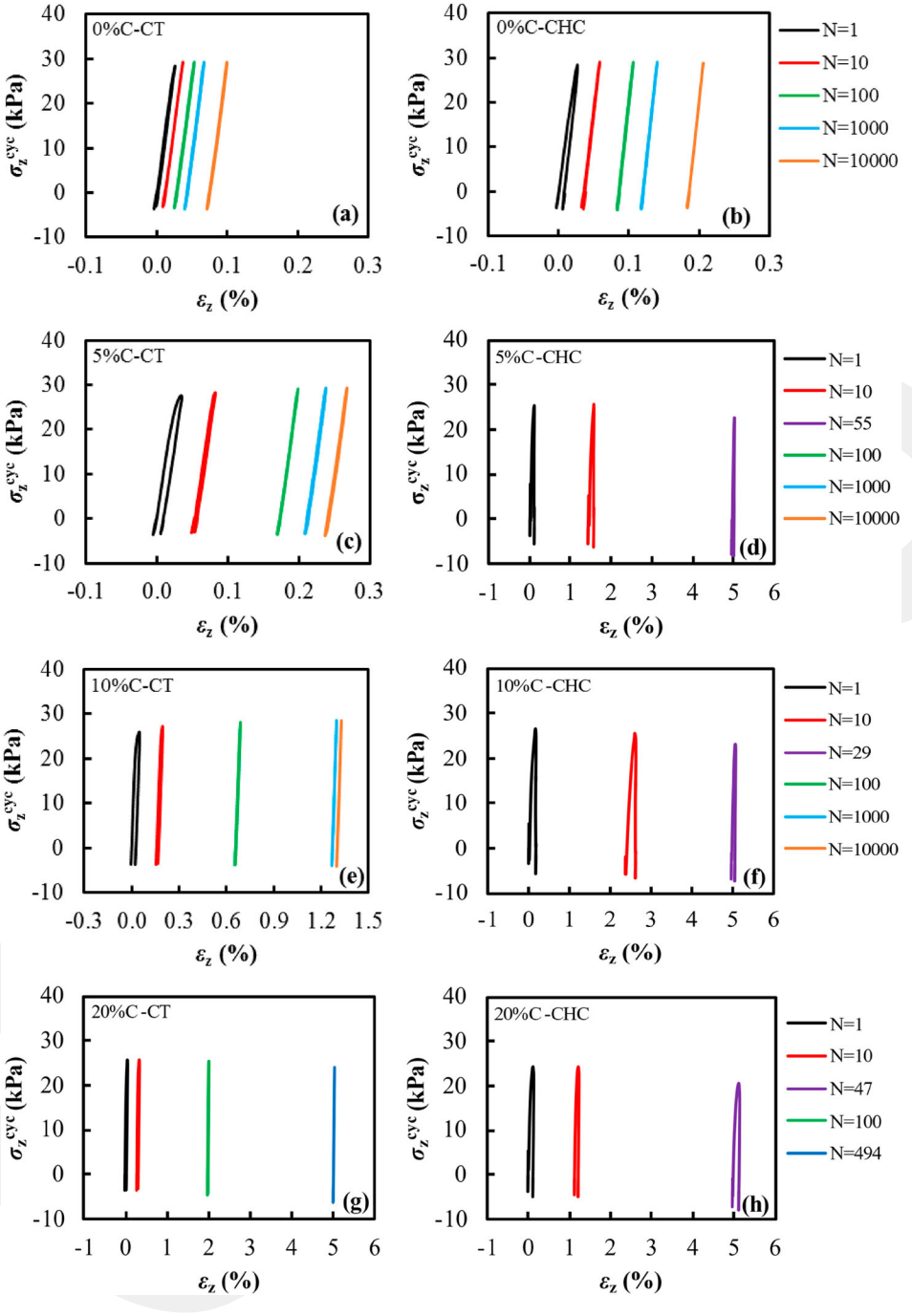

Figure 11. Axial stress versus axial strain for CT and CHC specimens at randomly load cycles: (a) CT-0% clay; (b) CHC-0% clay; (c) CT-5% clay; (d) CHC-5% clay; (e) CT-10% clay; (f) CHC-10% clay; (g) CT-20% clay and (h) CHC-20% clay.

as clay content raised. Figure 11 shows the typical examples of axial stress–strain loops at different numbers of cycles. It is also clearly seen in Figure 11 that the large part of axial strain developed within the first 1000 cycles for the specimens that did not fail during testing. Then, they produce a steadily growing axial strain over the whole test to reach their final strain. The failed CHC specimens produced

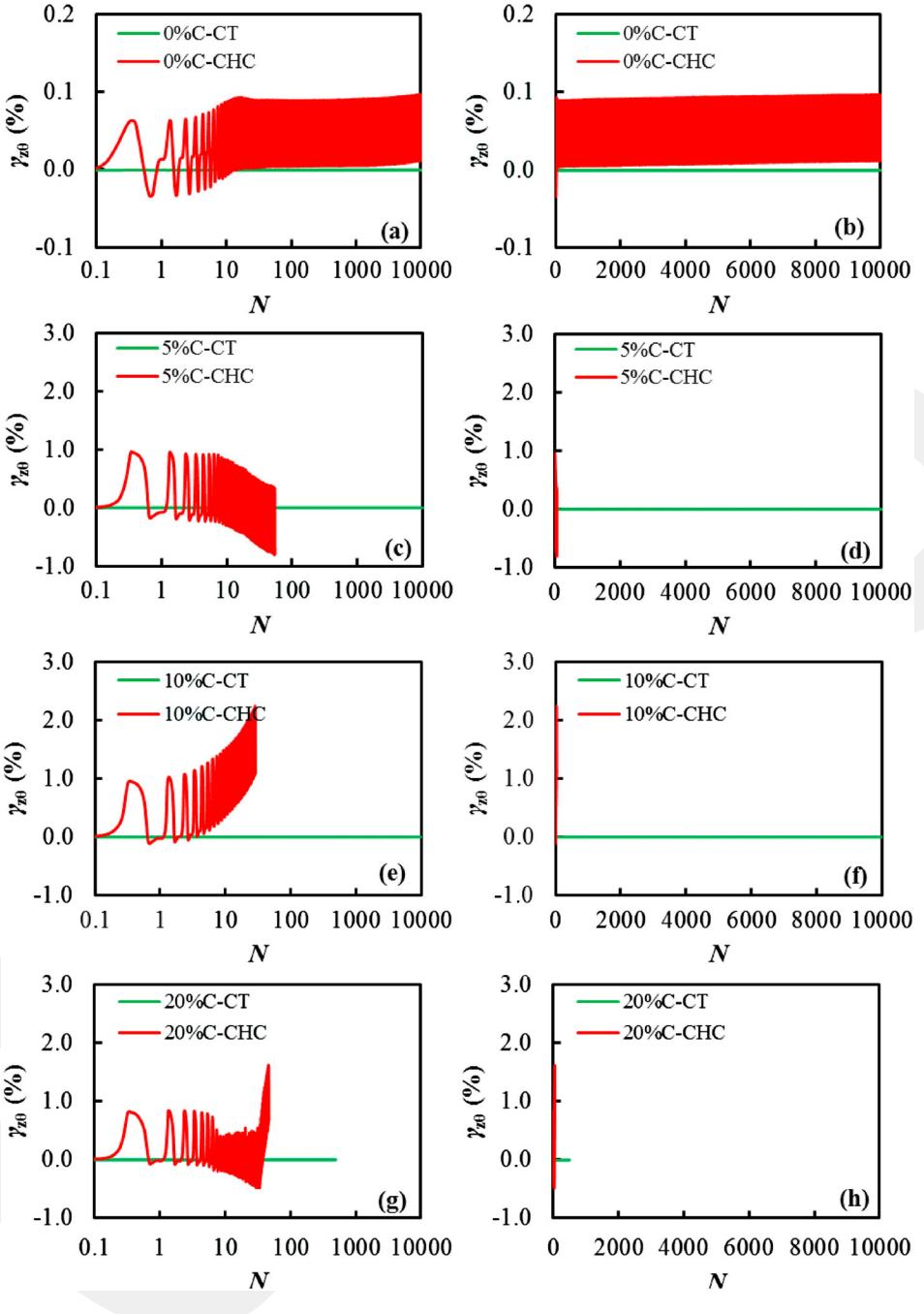

Figure 12. Shear strain versus number of load cycles for CT and CHC specimens: (a) 0% clay with logarithmic scale; (b) 0% clay without logarithmic scale; (c) 5% clay with logarithmic scale; (d) 5% clay without logarithmic scale; (e) 10% clay with logarithmic scale; (f) 10% clay without logarithmic scale; (g) 20% clay with logarithmic scale and (h) 20% clay without logarithmic scale.

an unstable behaviour under the heart-shaped stress path regardless of the clay contents (Figure 8). Thus, Figures 11(d, f, and h) show no meaningful relationships between axial stress–strain behaviour and clay contents at different load cycles for the specimens tested in this study.

3.4. Shear strain development

Shear strain development with the number of loading cycles in sand–clay mixtures under two different loading conditions (CT and CHC tests) is summarised in Figure 12. In order to clarify the shear strain development in earlier cycles of CHC tests, the horizontal axes in Figures 12(a, c, e, and g) were plotted in logarithmic scales. As mentioned earlier, all CT specimens were subjected to only cyclic axial load during shearing to mimic the loading condition of a CT testing system in the current study. As a result of this, all CT specimens yielded zero shear strain under cyclic loading (Figure 12). Figure 12 also shows that all CHC specimens produced higher shear strains due to the heart-shaped stress path involving torsional shear stress as well as axial stress. The degree of strain development due to a heart-shaped stress path in soils is affected by experimental parameters such as cyclic torsional stress ratio (η) (Cai et al., 2015, 2017, 2018; Guo et al., 2018). An increase in cyclic torsional stress ratio leads to an increase in the magnitude of principal stress rotation (α) (Figure 5). Therefore, it is expected that a specimen may exhibit a considerable shear strain in a CHC test depending on the increase in η. However, observation of this phenomenon was not within the scope of the current study; therefore, it was not investigated. The degree of shear strain development is also affected by the material types. For instance, sand materials may need a higher η since the interlocking of sand particles is likely to happen under loading, while clay materials can exhibit a similar shear strain performance with sand materials at a lower η. In this study, the sand–clay mixtures containing clay at different inclusion rates (0%, 5%, 10% and 20% clay by weight) were tested to investigate the effect of clay addition on the deformation behaviour of sand. Figures 12(a,b) present the results of shear strain development in the specimens without clay (0% clay) with the number of load cycles. It was clearly observed that the shear strain remained below 0.1% although the heart-shaped stress path led to an increase in shear strain. However, the specimens with clay yielded a higher shear strain at the same target cyclic torsional stress ratio. This behaviour can be explained that the clay addition decreased the interlocking of sand particles, which caused a

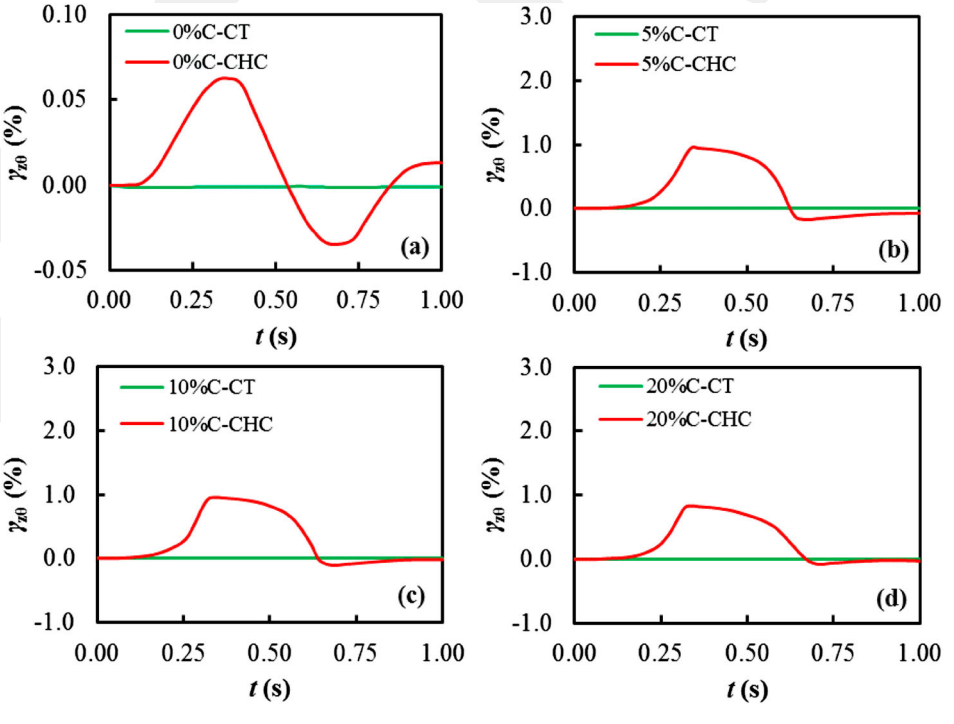

Figure 13. Shear strain development in CT and CHC specimens within one loading cycle: (a) 0% clay; (b) 5% clay; (c) 10% clay and (d) 20% clay.

reduction in the shear strength. Moreover, the target cyclic torsional stress ratio was determined to be high for sand–clay mixtures since they exhibited unstable behaviours for shear straining (Figure 12). As a result of this, a relationship between clay contents and shear strain was not detected. The unstable shear straining of CHC specimens is also presented in Figure 13. Figure 13 shows the shear strain development in all specimens in a single cycle. It can be claimed that only sand soil exhibited a similar pattern for shear strain with the waveform used for torsional shear stress in the CHC test (Figures 5–7). On the other hand, unstable patterns were observed for sand–clay mixtures with clay during CHC tests (Figures 12b–12d) regarding shear strain. This was also confirmed with the results presented in Figures 12(c–h).

3.5. Torsional shear stress–strain behavior

The test results regarding torsional shear stress–strain behaviour of CHC specimens are presented in Figure 14. In addition, a typical illustration of torsional shear stress–strain behaviours of CHC specimens for randomly selected two cycles is shown in Figure 15. Torsional shear stress was not applied on the specimens during CT tests; therefore, CT test results were not presented in Figures 14 and 15. It can be seen that the target amplitude for torsional shear stress was satisfactorily achieved in CHC sand only specimen. Furthermore, sand specimen exhibited a relatively linear behaviour and a stable pattern for torsional shear stress–strain response. As in the axial stress–strain behaviour, the loops shifted to the right by overlapping. The CHC specimen without clay generated lower shear straining under cyclic loads (Figure 14a). On the contrary, unstable patterns were observed for the torsional shear stress–strain behaviour of CHC sand–clay mixtures, regardless of clay contents (see Figures 14(b–d)). This was likely to occur due to the quick development of shear strain in soils with clay as a result of less interlocking of soil particles under a principal stress rotation. This also caused higher discrepancies in the amplitude of torsional shear stress.

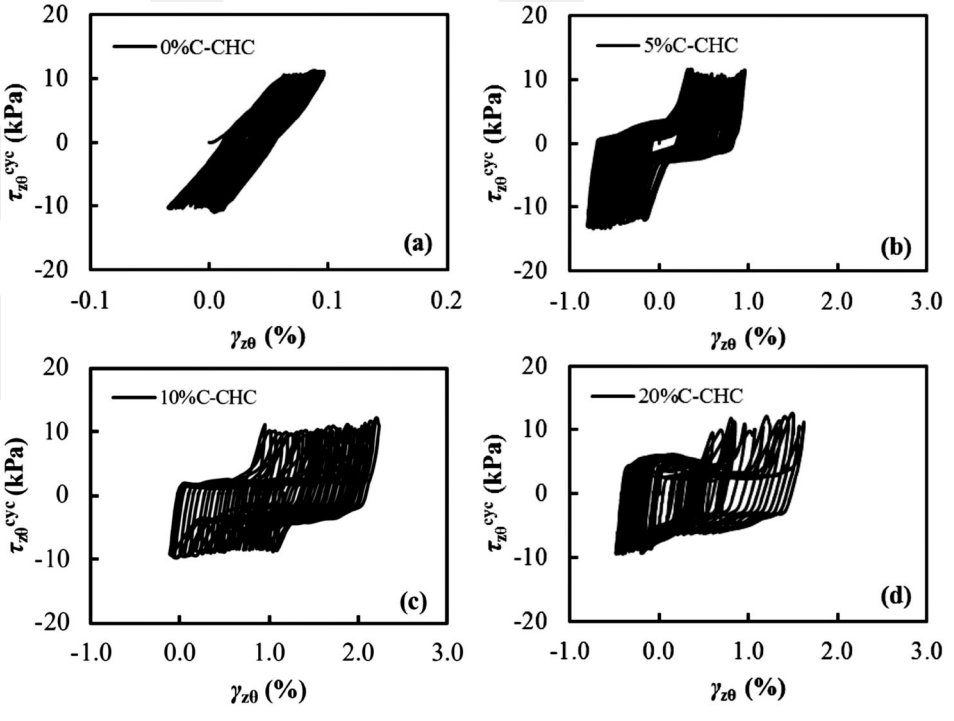

Figure 14. Shear stress versus shear strain for CHC specimens: (a) 0% clay; (b) 5% clay; (c) 10% clay and (d) 20% clay.

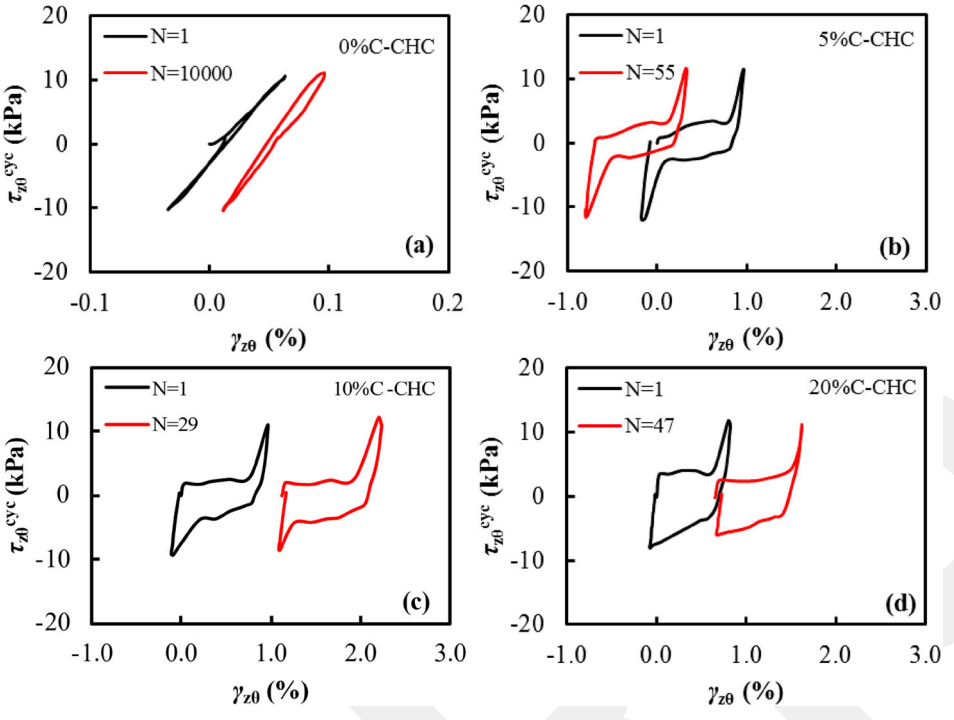

Figure 15. Shear stress versus shear strain for CHC specimens at randomly load cycles: (a) 0% clay; (b) 5% clay; (c) 10% clay and (d) 20% clay.

4. Conclusions

In this study, the response of dense sand–clay mixtures containing clay at the rates of 0%, 5%, 10% and 20% by weight under traffic loading was experimentally investigated regarding strain development and stress–strain behaviour. For this purpose, a series of cyclic triaxial (CT) and hollow cylinder (CHC) tests were carried out. From the test results, the following conclusions can be drawn:

(1) An axial strain development in sand increased after clay addition. This increment was determined to be affected by clay contents in CT tests. The CT specimens containing clay less than 20% carried the applied cyclic loads without failure ($\varepsilon_z < 5\%$) while the CT specimen containing 20% clay failed ($\varepsilon_z \geq 5\%$), which can be explained by the relatively high clay content.
(2) All CHC specimens with clay generated a quick development of axial strain and failed ($\varepsilon_z \geq 5\%$) in earlier cycles regardless of clay contents. This behaviour could be due to a PSR induced by a heart-shaped stress path and stress ratios used ($CVSR = 0.125$ and $\eta = 1/3$).
(3) A heart-shaped stress path caused a ratcheting behaviour in all CHC specimens with clay (5%, 10% and 20%) while ratcheting behaviour was observed in only CT specimen with 20% clay. That indicates that the PSR induced by a heart-shaped stress path should be considered to evaluate shakedown behaviour of dense sand–clay mixtures.
(4) The specimens without failure exhibited a strain-hardening behaviour. On the other hand, strain-softening behaviour was observed in failed specimens. Presence of clay and stress states of which specimens were subjected to may have resulted in this change in material behaviour.
(5) All specimens (except for the CHC specimen with 20% clay) exhibited a gradually decrease in distance between axial stress–strain loops with an increasing number of load cycles over the whole test. However, the CHC specimen with 20% clay exhibited a similar behaviour until $\varepsilon_z = 3\%$. After

$\varepsilon_z = 3\%$, this specimen generated the axial stress–strain loops with a gradually increasing distance. This behaviour (i.e. $\varepsilon_z > 3\%$) could be attributed to the less contact areas between sand particles due to a PSR and relatively high clay content (20% in this study).

(6) All CT specimens produced zero shear strain since no torsional shear stress was applied in the CT tests of this study. Unlike CT tests, both axial stress and torsional shear stress were cyclically imposed on all CHC specimens to achieve a heart-shaped stress path. As a result, the torsional shear stress led to shear strain development in CHC specimens.

(7) For the torsional shear stress–strain responses, a CHC specimen without clay exhibited a relatively linear behaviour and produced a stable pattern. The loops nearly coincided and a gradual decrease in distance between the loops was observed with an increasing number of loading cycles. On the contrary, unstable patterns for the torsional shear stress–strain behaviour were observed in all CHC specimens including clay regardless of clay content. This behaviour could be explained by a quick development of shear strain in earlier cycles due to the heart-shaped stress path and magnitude of η used.

(8) The CT tests not including PSR with sudden 90-degree changes in the principal stress direction underestimated the permanent strain in dense sand–clay mixtures, which may result in inadequate design and structural failure of pavement systems. Based on the findings of this study, it is recommended that a PSR induced by traffic load be taken into consideration when investigating deformation behaviour of dense sand–clay mixtures containing clay at low rates ($\leq 20\%$).

Acknowledgement

The first author would like to thank the Scientific and Technological Research Council of Turkey (TUBITAK) for the financial support of his postdoctoral research at the Department of Civil, Construction and Environmental Engineering, Iowa State University.

Disclosure statement

No potential conflict of interest was reported by the author(s).

Data Availability Statement

The authors confirm that the data supporting the findings of this study are available within the article.

ORCID

Halil Ibrahim Fedakar http://orcid.org/0000-0002-7561-5363
Bora Cetin http://orcid.org/0000-0003-0415-7139

References

Alnedawi, A., Nepal, K. P., & Al-Ameri, R. (2018). Mechanistic behavior of open and dense graded unbound granular materials under traffic loads. *International Journal of GEOMATE*, *14*(45), 124–129. https://doi.org/10.21660/2018.45.7336

Alnedawi, A., Nepal, K. P., & Al-Ameri, R. (2021). Effect of loading frequencies on permanent deformation of unbound granular materials. *International Journal of Pavement Engineering*, *22*(8), 1008–1016. https://doi.org/10.1080/10298436.2019.1656807

Cai, Y. Y. (2010). *An experimental study of non-coaxial behavior using hollow cylinder testing* [Doctoral dissertation, University of Nottingham]. Nottingham eTheses. http://eprints.nottingham.ac.uk/11214/

Cai, Y. Q., Guo, L., Jardine, R. J., Yang, Z. X., & Wang, J. (2017). Stress-strain response of soft clay to traffic loading. *Géotechnique*, *67*(5), 446–451. https://doi.org/10.1680/jgeot.15.P.224

Cai, Y. Q., Sun, Q., Guo, L., Juang, C. H., & Wang, J. (2015). Permanent deformation characteristics of saturated sand under cyclic loading. *Canadian Geotechnical Journal*, *52*(6), 795–807. https://doi.org/10.1139/cgj-2014-0341

Cai, Y., Wu, T., Guo, L., & Wang, J. (2018). Stiffness degradation and plastic strain accumulation of clay under cyclic load with principal stress rotation and deviatoric stress variation. *Journal of Geotechnical and Geoenvironmental Engineering*, *144*(5), 04018021. https://doi.org/10.1061/(ASCE)GT.1943-5606.0001854

Cetin, A., Kaya, Z., Cetin, B., & Aydilek, A. H. (2014). Influence of laboratory compaction method on mechanical and hydraulic characteristics of unbound granular base materials. *Road Materials and Pavement Design*, *15*(1), 220–235. https://doi.org/10.1080/14680629.2013.869505

Chai, J. C., & Miura, N. (2002). Traffic-load-induced permanent deformation of road on soft subsoil. *Journal of Geotechnical and Geoenvironmental Engineering*, *128*(11), 907–916. https://doi.org/10.1061/(ASCE)1090-0241(2002)128:11(907)

Chazallon, C., Hornych, P., & Mouhoubi, S. (2006). Elastoplastic model for the long-term behavior modeling of unbound granular materials in flexible pavements. *International Journal of Geomechanics*, *6*(4), 279–289. https://doi.org/10.1061/(ASCE)1532-3641(2006)6:4(279)

Cheung, L. W. (1994). *Laboratory assessment of pavement foundation materials* [Doctoral. dissertation, University of Nottingham]. Nottingham eTheses. http://eprints.nottingham.ac.uk/10944/

Cui, Y. J. (2018). Mechanical behaviour of coarse grains/fines mixture under monotonic and cyclic loadings. *Transportation Geotechnics*, *17*(A), 91–97. https://doi.org/10.1016/j.trgeo.2018.09.016

Fedakar, H. I., Cai, W., Rutherford, C. J., & Çetin, B. (2020). Evaluation of deformation behavior of sand-clay mixture under traffic loads. *In Proceedings of Geo-Congress 2020: Vision, Insight, Outlook*, 201–209. Minnesota, USA. https://doi.org/10.1061/9780784482803.022

Frost, M. W., Fleming, P. R., & Rogers, C. D. F. (2004). Cyclic triaxial tests on clay subgrades for analytical pavement design. *Journal of Transportation Engineering*, *130*(3), 378–386. https://doi.org/10.1061/(ASCE)0733-947X(2004)130:3(378)

Gao, H., Bu, C., Wang, Z., Shen, Y., & Chen, G. (2017). Dynamic characteristics of expanded polystyrene composite soil under traffic loadings considering initial consolidation state. *Soil Dynamics and Earthquake Engineering*, *102*, 86–98. https://doi.org/10.1016/j.soildyn.2017.08.012

Georgiannou, V. N., & Konstadinou, M. (2014). Effects of density on cyclic behaviour of anisotropically consolidated Ottawa sand under undrained torsional loading. *Géotechnique*, *64*(4), 287–302. https://doi.org/10.1680/geot.13.P.090

Gräbe, P. J. (2002). *Resilient and permanent deformation of railway foundations under principal stress rotation* [Doctoral dissertation, University of Southampton].

Gräbe, P. J., & Clayton, C. R. (2009). Effects of principal stress rotation on permanent deformation in rail track foundations. *Journal of Geotechnical and Geoenvironmental Engineering*, *135*(4), 555–565. https://doi.org/10.1061/(ASCE)1090-0241(2009)135:4(555)

Guimarães, A. C. R., da Motta, L. M. G., & Castro, C. D. (2019). Permanent deformation parameters of fine-grained tropical soils. *Road Materials and Pavement Design*, *20*(7), 1664–1681. https://doi.org/10.1080/14680629.2018.1473283

Guo, L., Cai, Y., Jardine, R. J., Yang, Z., & Wang, J. (2018). Undrained behaviour of intact soft clay under cyclic paths that match vehicle loading conditions. *Canadian Geotechnical Journal*, *55*(1), 90–106. https://doi.org/10.1139/cgj-2016-0636

Guo, L., Chen, J., Wang, J., Cai, Y., & Deng, P. (2016). Influences of stress magnitude and loading frequency on cyclic behavior of K_0-consolidated marine clay involving principal stress rotation. *Soil Dynamics and Earthquake Engineering*, *84*, 94–107. https://doi.org/10.1016/j.soildyn.2016.01.024

Haider, I., Kaya, Z., Cetin, A., Hatipoglu, M., Cetin, B., & Aydilek, A. H. (2014). Drainage and mechanical behavior of highway base materials. *Journal of Irrigation and Drainage Engineering*, *140*(6), 04014012. https://doi.org/10.1061/(ASCE)IR.1943-4774.0000708

Hight, D. W., Gens, A., & Symes, M. J. (1983). The development of a new hollow cylinder apparatus for investigating the effects of principal stress rotation in soils. *Géotechnique*, *33*(4), 355–383. https://doi.org/10.1680/geot.1983.33.4.355

Hyodo, M., Murata, H., Yasufuku, N., & Fujii, T. (1991). Undrained cyclic shear strength and residual shear strain of saturated sand by cyclic triaxial tests. *Soils and Foundations*, *31*(3), 60–76. https://doi.org/10.3208/sandf1972.31.3_60

Hyodo, M., Yamamoto, Y., & Sugiyama, M. (1994). Undrained cyclic shear behaviour of normally consolidated clay subjected to initial static shear stress. *Soils and Foundations*, *34*(4), 1–11. https://doi.org/10.3208/sandf1972.34.4_1

Ishihara, K. (1996). *Soil behavior in earthquake geotechnics*. Clarendon Press.

Kim, D., & Kim, J. R. (2007). Resilient behavior of compacted subgrade soils under the repeated triaxial test. *Construction and Building Materials*, *21*(7), 1470–1479. https://doi.org/10.1016/j.conbuildmat.2006.07.006

Korkiala-Tanttu, L., & Dawson, A. (2007). Relating full-scale pavement rutting to laboratory permanent deformation testing. *International Journal of Pavement Engineering*, *8*(1), 19–28. https://doi.org/10.1080/10298430600783509

Li, L., Dan, H., & Wang, L. (2011). Undrained behavior of natural marine clay under cyclic loading. *Ocean Engineering*, *38*(16), 1792–1805. https://doi.org/10.1016/j.oceaneng.2011.09.004

Li, L., Liu, J., Zhang, X., Li, P., & Saboundjian, S. (2019). Characterizing permanent deformation of Alaskan granular base-course materials. *Journal of Materials in Civil Engineering*, *31*(11), 04019267. https://doi.org/10.1061/(ASCE)MT.1943-5533.0002911

Mamou, A. (2013). *Effects of principal stress rotation and drainage on the resilient stiffness of railway foundations* [Doctoral dissertation, University of Southampton].

Mamou, A., Priest, J. A., Clayton, C. R. I., & Powrie, W. (2018). Behaviour of saturated railway track foundation materials during undrained cyclic loading. *Canadian Geotechnical Journal*, *55*(5), 689–697. https://doi.org/10.1139/cgj-2017-0196

Noolu, V., Mudavath, H., Pillai, R. J., & Yantrapalli, S. K. (2019). Permanent deformation behaviour of black cotton soil treated with calcium carbide residue. *Construction and Building Materials*, *223*, 441–449. https://doi.org/10.1016/j.conbuildmat.2019.07.010

Pradhan, T. B. S., Tatsuoka, F., & Horii, N. (1988). Simple shear testing on sand in a torsional shear apparatus. *Soils and Foundations*, *28*(2), 95–112. https://doi.org/10.3208/sandf1972.28.2_95

Puppala, A. J., Mohammad, L. N., & Allen, A. (1999). Permanent deformation characterization of subgrade soils from RLT test. *Journal of Materials in Civil Engineering*, *11*(4), 274–282. https://doi.org/10.1061/(ASCE)0899-1561(1999)11:4(274)

Puppala, A. J., Saride, S., & Chomtid, S. (2009). Experimental and modeling studies of permanent strains of subgrade soils. *Journal of Geotechnical and Geoenvironmental Engineering*, *135*(10), 1379–1389. https://doi.org/10.1061/(ASCE)GT.1943-5606.0000163

Qian, J. G., Wang, Y. G., Yin, Z. Y., & Huang, M. S. (2016). Experimental identification of plastic shakedown behavior of saturated clay subjected to traffic loading with principal stress rotation. *Engineering Geology*, *214*, 29–42. https://doi.org/10.1016/j.enggeo.2016.09.012

Saada, A. (1988). State-of-the-art paper: Hollow cylinder torsional devices: Their advantages and limitations. In R. T. Donaghe, R. C. Chaney, & M. L. Silver (Eds.), *Advanced triaxial testing of soil and rock, ASTM STP977* (pp. 766–795). ASTM.

Saberian, M., & Li, J. (2019). Long-term permanent deformation behaviour of recycled concrete aggregate with addition of crumb rubber in base and sub-base applications. *Soil Dynamics and Earthquake Engineering*, *121*, 436–441. https://doi.org/10.1016/j.soildyn.2019.03.029

Saberian, M., Li, J., & Setunge, S. (2019). Evaluation of permanent deformation of a new pavement base and subbase containing unbound granular materials, crumb rubber and crushed glass. *Journal of Cleaner Production*, *230*, 38–45. https://doi.org/10.1016/j.jclepro.2019.05.100

Shen, Y., Wang, X., Liu, H. L., Du, W. H., Wang, B. G., & Xu, H. D. (2017). Influence of principal stress rotation of unequal tensile and compressive stress amplitudes on characteristics of soft clay. *Journal of Mountain Science*, *14*(2), 369–381. https://doi.org/10.1007/s11629-016-4000-9

Shibuya, S. (1988). A servo system for hollow cylinder testing of soils. *Geotechnical Testing Journal*, *11*(2), 109–118. https://doi.org/10.1520/GTJ10956J

Simpson, D. C., & Evans, T. M. (2016). Behavioral thresholds in mixtures of sand and kaolinite clay. *Journal of Geotechnical and Geoenvironmental Engineering*, *142*(2), 04015073. https://doi.org/10.1061/(ASCE)GT.1943-5606.0001391

Tatsuoka, F., Sonoda, S., Hara, K., Fukushima, S., & Pradhan, T. B. S. (1986). Failure and deformation of sand in torsional shear. *Soils and Foundations*, *26*(4), 79–97. https://doi.org/10.3208/sandf1972.26.4_79

Vaid, Y. P., & Chern, J. C. (1983). Effect of static shear on resistance to liquefaction. *Soils and Foundations*, *23*(1), 47–60. https://doi.org/10.3208/sandf1972.23.47

Vaid, Y. P., Sayao, A., Hou, E., & Negussey, D. (1990). Generalized stress-path-dependent soil behaviour with a new hollow cylinder torsional apparatus. *Canadian Geotechnical Journal*, *27*(5), 601–616. https://doi.org/10.1139/t90-075

Wang, Y., Gao, Y., Guo, L., & Yang, Z. (2018). Influence of intermediate principal stress and principal stress direction on drained behavior of natural soft clay. *International Journal of Geomechanics*, *18*(1), 04017128. https://doi.org/10.1061/(ASCE)GM.1943-5622.0001042

Xiong, H., Guo, L., Cai, Y. Q., & Yang, Z. X. (2016). Experimental study of drained anisotropy of granular soils involving rotation of principal stress direction. *European Journal of Environmental and Civil Engineering*, *20*(4), 431–454. https://doi.org/10.1080/19648189.2015.1039662

Yang, Q., Tang, Y., Yuan, B., & Zhou, J. (2019). Cyclic stress-strain behaviour of soft clay under traffic loading through hollow cylinder apparatus: Effect of loading frequency. *Road Materials and Pavement Design*, *20*(5), 1026–1058. https://doi.org/10.1080/14680629.2018.1428219